Chapter 4

Simulation Results

This chapter provides an overview of the results obtained while implementing and integrating the various sub-modules of the renewable energy system.

A quantitative approach was followed while generating the simulation results of the various modules where the same amount of attention was paid to rare phenomena as to frequently expected results. A case study was performed for a site in Alexander bay in South Africa in order to demonstrate the functionality of the various modules. Wind data from the WASA project was employed along with solar data from NASA's solar irradiance data file for this site located at a latitude of -28.583333, and longitude 16.483333 [46]. This is a lesser known format for the Global Positioning System (GPS) coordinates that is usually expressed in the format of $degrees^{\circ} : minutes' : seconds''$, but for this simulation the format containing only degrees was required.

4.1 Model results

4.1.1 Optimal tilt

The tilt angle calculated by this module is based upon the premise that a fixed tilt PV panel array will be used for the system. The optimal tilt module calculated that the optimal tilt angle for a PV panel in Alexander bay is equal to 50°. The incident solar irradiance for a tilt of 0° is shown in red on figure 4.1, while the white graph represents the solar irradiation values for the optimal tilt angle. The last curve present on this figure represents the insolation values for a manual tilt angle of 15°. It is clear that during certain months of the year, this manual tilt angle will receive substantially more solar irradiance than the optimal tilt angle, but will receive substantially less for the remainder of the year. Thus the optimal tilt angle ensures that the maximum solar irradiation is received during the worst month of the year.

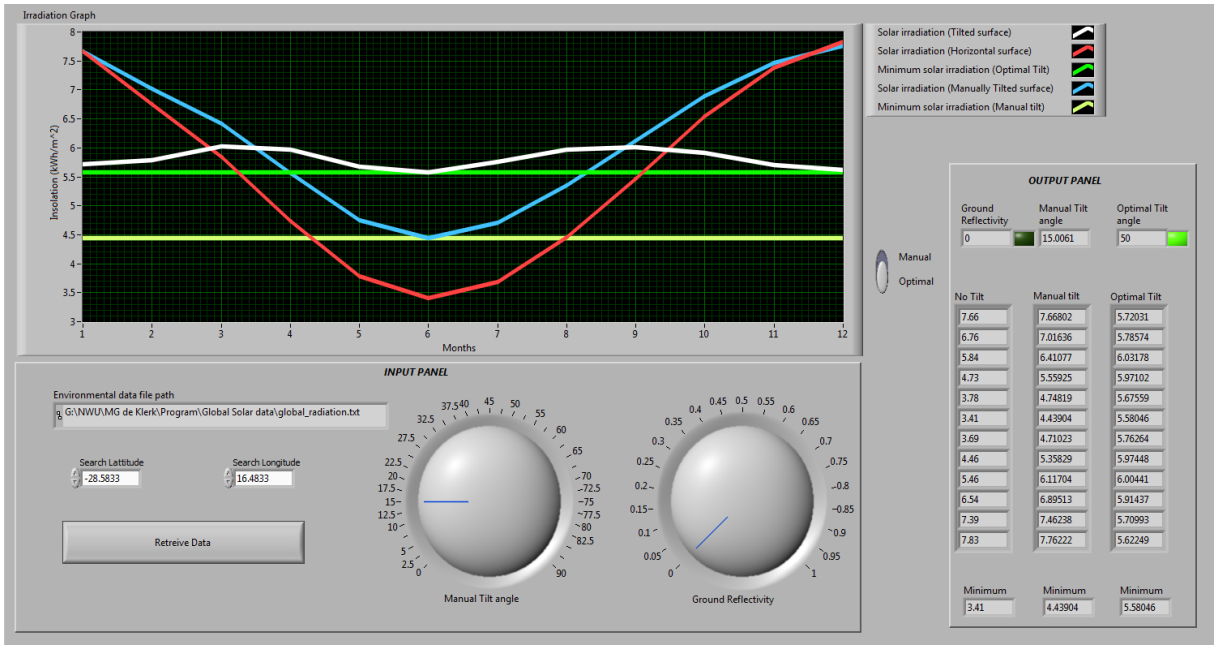

Figure 4.1: Optimum tilt interface

The greater the tilt angle, the greater the effect of ground reflectivity on the incident solar irradiation. The greater the ground reflectivity due to e.g. snow or a silver roof,

the more solar irradiation will be reflected back towards the PV panel. Thus the ground reflectivity effect increases the incident solar irradiance for all months of the year by a small amount.

4.1.2 PV Panels

Manufacturers tend to classify their PV panels according to the power output achieved during tests done under the conditions of the nominal terrestrial environment (NTE) as expressed in section 2.3.1, usually with an error margin of $\pm 10\%$. This power output deviation is further compounded when the environment differs from the NTE, most noticeably, the temperature and solar irradiance values. The PV panel model implemented in LabView takes the environmental variables into account and calculated the probable power output of the PV panel for the location by using the techniques and equations as set forth in section 3.3.1.

After supplying all of the PV panel's parameters, as found in the PV panel's technical data sheet, to the model manually or by loading stored parameters from file, the model calculates the probable power output of the PV panel. As a precaution, the PV panel model chooses the lowest value between the specified irradiance (G_{ref}) in the NTE, and the hourly irradiance on a tilted surface (G_T). This was done for various reasons:

- It is probable that when supplied with more solar irradiation than what was received during testing under NTE conditions, that the panel will provide more power than what it was rated for. The problem with this principle is that the extent of this over-exposure power is not specified and the device will reach saturation at some stage, thus provide a false power value that doesn't correlate with actual values.
- By not taking this additional power into account during the initial system design phase, it may be beneficial during the systems' life span. The extra power that may be generated in this over-exposed state will help to reduce the perceived loss of efficiency due to dust and dirt as well as solar degradation of the PV panel.

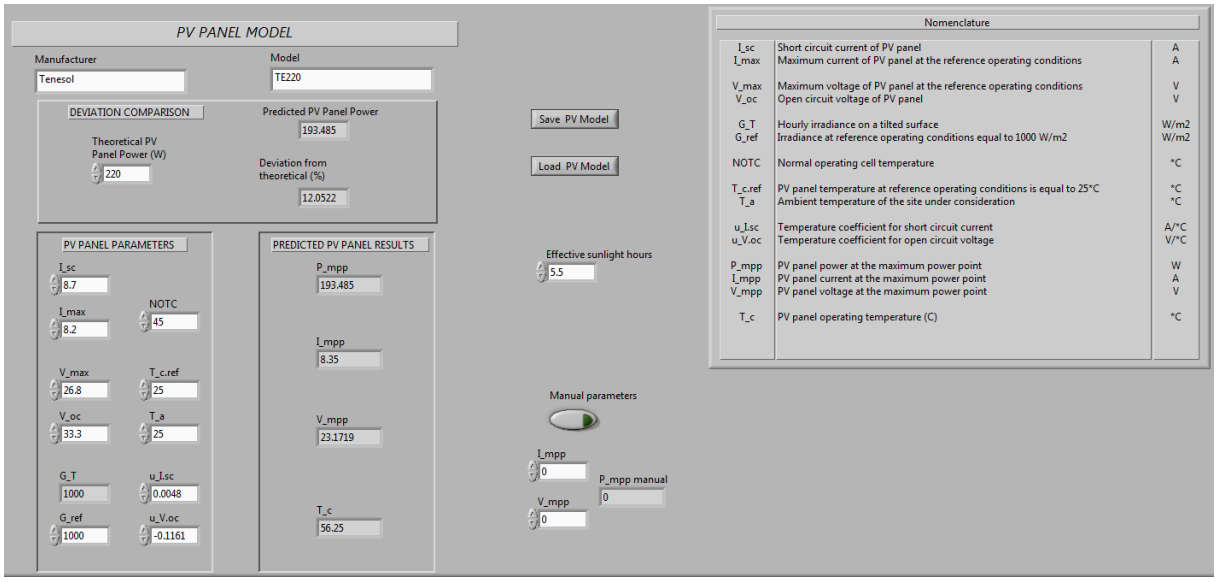

Figure 4.2: PV panel user interface

A screen shot of the PV panel module's user interface, populated with the parameters of a Tenesol TE220 PV panel, is show in figure 4.2. The simulation results for this PV panel with an ambient temperature of 25°*C* (equal to the test environment) and 35°*C* is summarized in table 4.1, as well as the results for a different PV panel model. One can clearly see that an increase in temperature, has a detrimental effect on the power output of the PV panel.

These results were verified in the Matlab environment and delivered the same results. It is important to note that these values were consistently lower than the values promoted in the PV panel's data sheet [47]. Multiple panel simulations indicated that

Table 4.1: PV panel power output comparison

MAKE	***MODEL***	***AMBIENT TEMP***	***RATED POWER (W)***	***PREDICTED POWER (W)***	***DEVIATION %***
Tenesol	TE190	25	190	165.633	12.8249
	TE190	30	190	161.633	14.9301
Tenesol	TE220	25	220	193.485	12.0522
	TE220	30	220	189.180	14.0090

the implemented PV panel module delivers a conservative output that is between 10% and 15% lower than the values claimed by the manufacturers in their data sheets as seen in table 4.1. The irradiance value for G_T was calculated by the optimal tilt module in section 4.1.1.

4.1.3 PV panel array shading

From figure 2.4, we could establish that Alexander Bay is located in a low latitude region, hence a set back ratio of 2 should be used in the calculations. By supplying the length and width of the PV panel to be used, the module could calculate the rest of the parameters, including the horizontal distance $(d_{horizontal})$ between rows required to prevent shading. This module is only executed after the optimal tilt calculations have been completed, as this tilt value is required for the shading calculations.

The PV panel array shading module calculates the effective distances required to prevent accidental shading of the PV panels by neighbouring PV panels. Figure 4.3 shows the effective ground cover ratio (GCR) per panel to prevent shading. It is interesting to note how much larger the area required for the array will be if shading is taken into account - 1.4925m^2 compared to 3.246m^2 when compensating for shading with a SBR of 2.

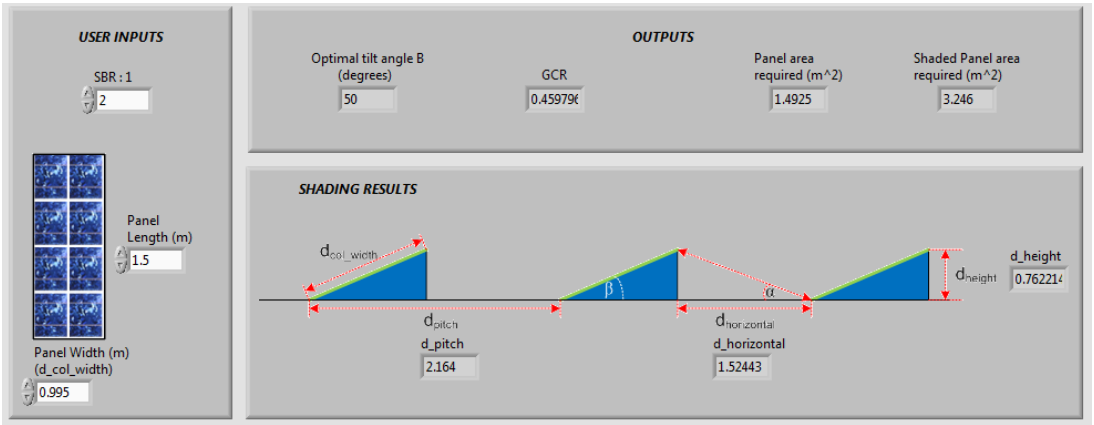

Figure 4.3: Screen capture of the PV array shading module

4.1.4 Wind analysis

The main idea behind the wind analysis module was to analyse the data for a certain site in order to determine the amount of power that can be extracted by a wind turbine. It was decided to implement the Weibull PDF estimation technique to model the wind in order to simplify further calculations. The first step towards calculating the Weibull PDF, was to calculate the shape and scale parameters of the data set in question. Data for multiple years from the WASA project's WM01 site - Alexander bay - was used to perform the wind analysis. The wind data at a height of 62 meters was used for all wind calculations.

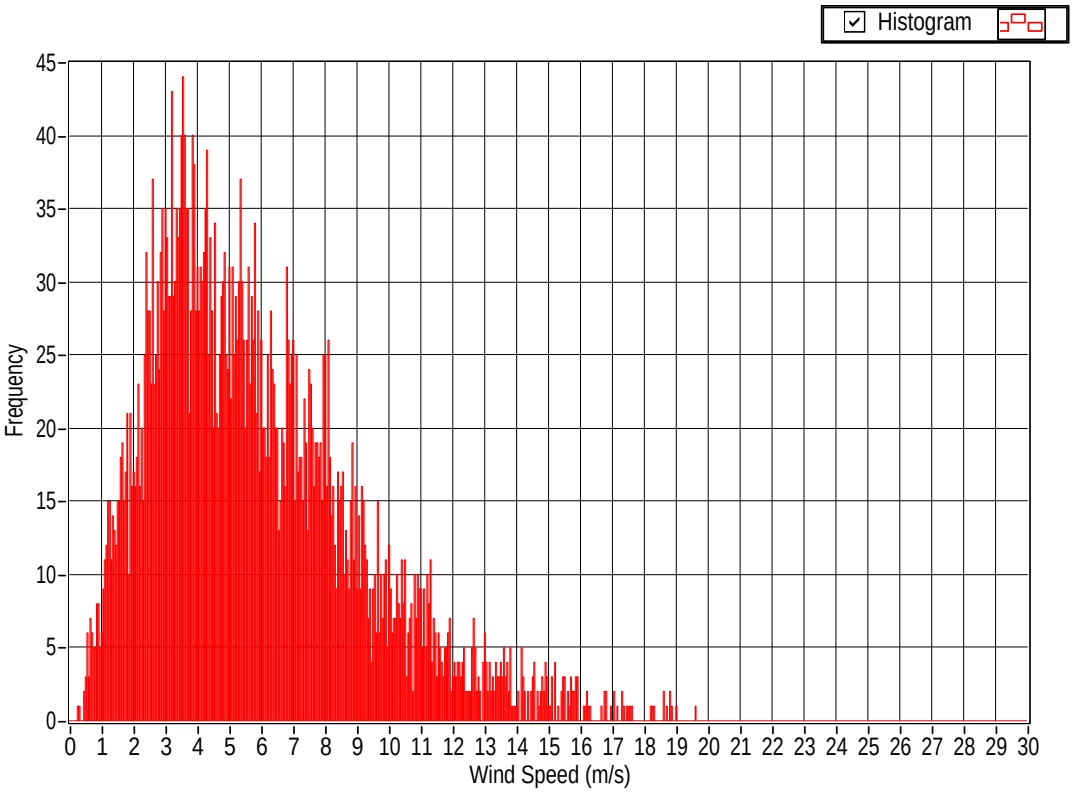

Figure 4.4: Raw data histogram for Site WM01 for the month of December

First up was the maximum likelihood estimation (MLE) method from section 2.4.2. The MLE method was implemented, but was found to be a computational and time intensive method as shown in table 3.5, resulting in an alternative method being implemented alongside the MLE method. This alternative method, referred to as the

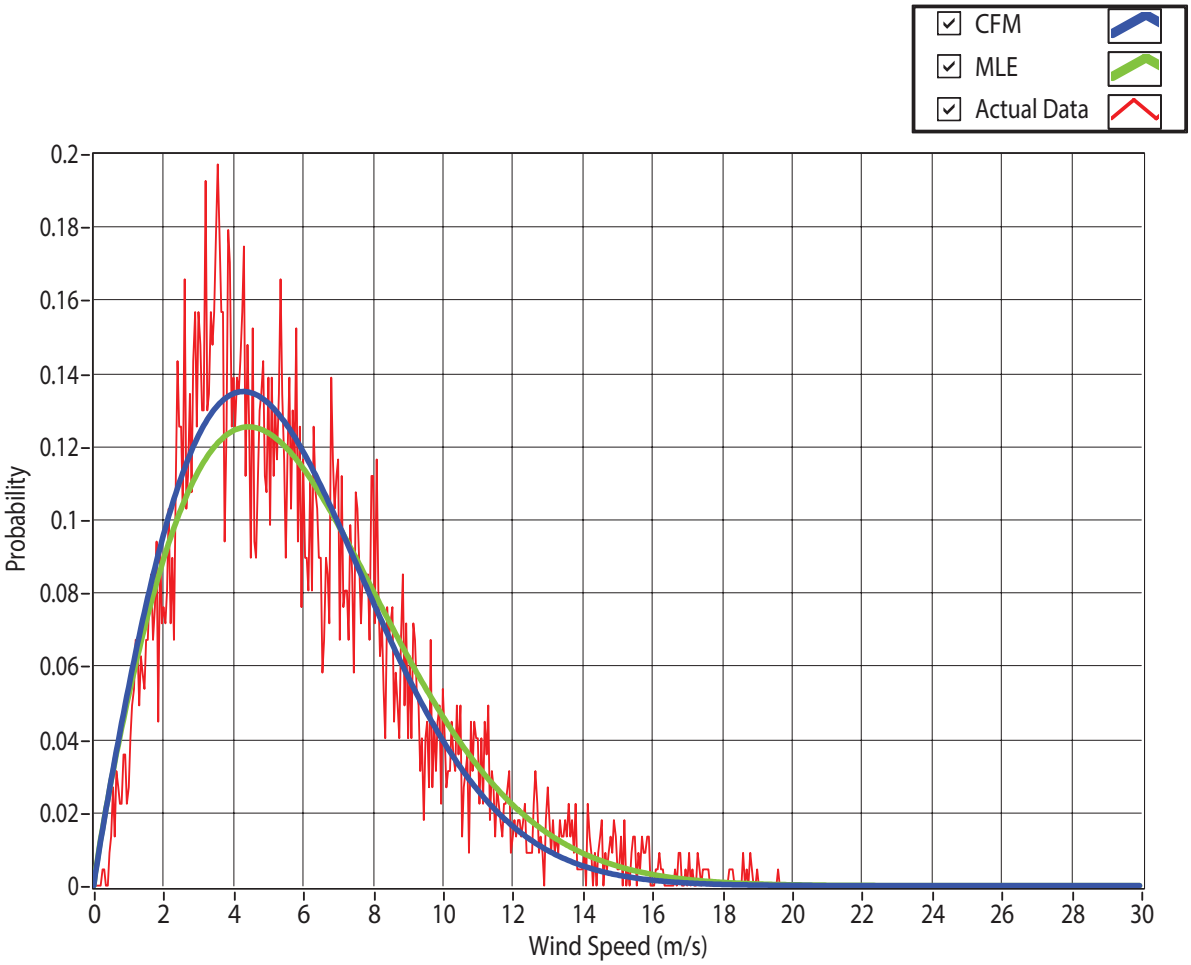

Figure 4.5: Comparison of MLE and CFM Weibull curves

curve fit method (CFM), was included in the simulation model to provide a quick preliminary analysis of the data with the option to perform the more time consuming MLE analysis afterwards at the user's discretion.

As described in section 3.4.2, the CFM requires a histogram of the raw data. This histogram with a bin width of $0.05\frac{m}{s}$ was generated from the raw data and displayed in figure 4.4. The parameters of the Weibull curve that was the best fit to the histogram's envelope, was determined and is illustrated in figure 4.5 alongside the Weibull curve based upon the MLE's parameters. Please note the change of the Y-axis between figure 4.4 and figure 4.5. The envelope of the histogram in figure 4.5 has been normalised relative to the number of data entries in the data set for the given month

by implementing equation 3.26.

The results of both the MLE method and the CFM are compared in table 4.2 as well as the differences between the respective results. For this case study, the maximum difference was found in July with a difference of 9.718%. This difference $D_{\%}$ was calculated relative to the average of the two parameters obtained from the various methods with the help of the following equation:

$$D_{\%} = \frac{\left|CFM_p - MLE_p\right|}{\left(\frac{CFM_p + MLE_p}{2}\right)} \tag{4.1}$$

where the subscript $_p$ represents either the shape or the scale parameter of each method.

The average differences between the raw data's normalised histogram and the Weibull curves are listed in table 4.3 in order to verify the goodness of fit of the Weibull curves to the raw data. In figure 4.5 one can see that there is a slight difference between the MLE and CFM Weibull PDFs, but they still provide a good approximation of the data set.

4.1.5 Wind turbine

The probability of encountering each wind speed has been estimated with the Weibull PDF in the preceding section. The next stage of the simulation model required a mathematical representation of the wind turbine's power curve. This wind turbine model will be combined with the Weibull PDF in order to calculate the probable power output of the wind turbine based upon these wind speed values.

Various techniques were implemented resulting in power curves as shown in figure 3.4, but the 6th order polynomial as illustrated in figure 4.7, provided the best approximation for the turbine's power curve seen in figure 4.6.

Table 4.2: Weibull parameters comparison

MONTH	***CFM***		***MLE***		***DIFF***		***DIFF %***	
	Shape	*Scale*	*Shape*	*Scale*	*Shape*	*Scale*	*Shape*	*Scale*
Jan	1.686	6.393	1.695	6.683	0.009	0.290	0.552	4.431
Feb	1.568	5.802	1.674	5.882	0.106	0.080	6.526	1.373
Mar	1.542	5.844	1.577	6.201	0.035	0.356	2.243	5.919
Apr	1.488	6.001	1.560	6.192	0.071	0.191	4.671	3.129
May	1.655	5.248	1.702	5.534	0.047	0.285	2.799	5.295
Jun	1.714	6.135	1.824	6.199	0.110	0.063	6.246	1.029
Jul	1.808	8.276	1.993	7.554	0.185	0.722	9.718	9.123
Aug	1.626	6.076	1.668	6.331	0.042	0.255	2.529	4.111
Sep	1.659	6.550	1.725	6.689	0.066	0.139	3.890	2.101
Oct	1.749	6.755	1.822	6.975	0.072	0.220	4.044	3.202
Nov	1.646	7.097	1.687	7.273	0.041	0.175	2.440	2.441
Dec	1.939	6.227	1.889	6.599	0.050	0.373	2.638	5.812

Table 4.3: CFM and MLE Weibull curve deviations from the raw data histogram

MONTH	***CFM***	***MLE***
Jan	0.00856825	0.00184144
Feb	0.00848454	0.00201015
Mar	0.00865706	0.0023313
Apr	0.0080255	0.00170549
May	0.0085473	0.00228994
Jun	0.00723385	0.00191825
Jul	0.0123894	0.00510942
Aug	0.00810165	0.00177779
Sep	0.00888224	0.0013678
Oct	0.00903515	0.00174053
Nov	0.00795668	0.00117152
Dec	0.0074091	0.00280499
AVERAGE	*0.00860756*	*0.002172385*

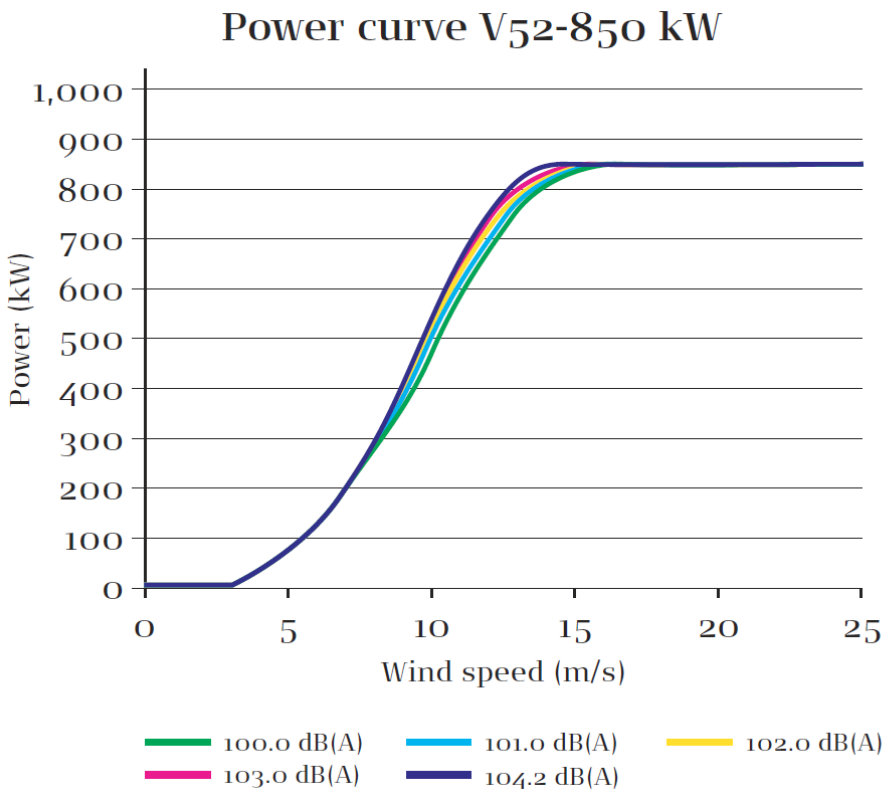

Figure 4.6: Power curve of a Vestas V52-850kW wind turbine at different sound levels [11]

After re-creating the actual turbine's power curve seen in figure 4.6 in Microsoft Excel, we were able to fit a 6th-order polynomial curve through the data. The coefficients of this fitted curve was then supplied to the wind turbine module to re-create the actual wind turbine's power curve. This resulted in a power curve as illustrated in figure 4.7, with the polynomial represented by:

$$P(v) = -0.1616v^6 + 13.887v^5 - 435.21v^4 + 5779.7v^3 - 26522v^2 + 38170v. \quad (4.2)$$

The polynomial provides a good representation of the transient phase $(v_c i \rightarrow v_r)$ and most of the rated phase of the wind turbine's power curve, but it is important to still enforce the cut-in and cut-out velocities of the turbine explicitly in the model.

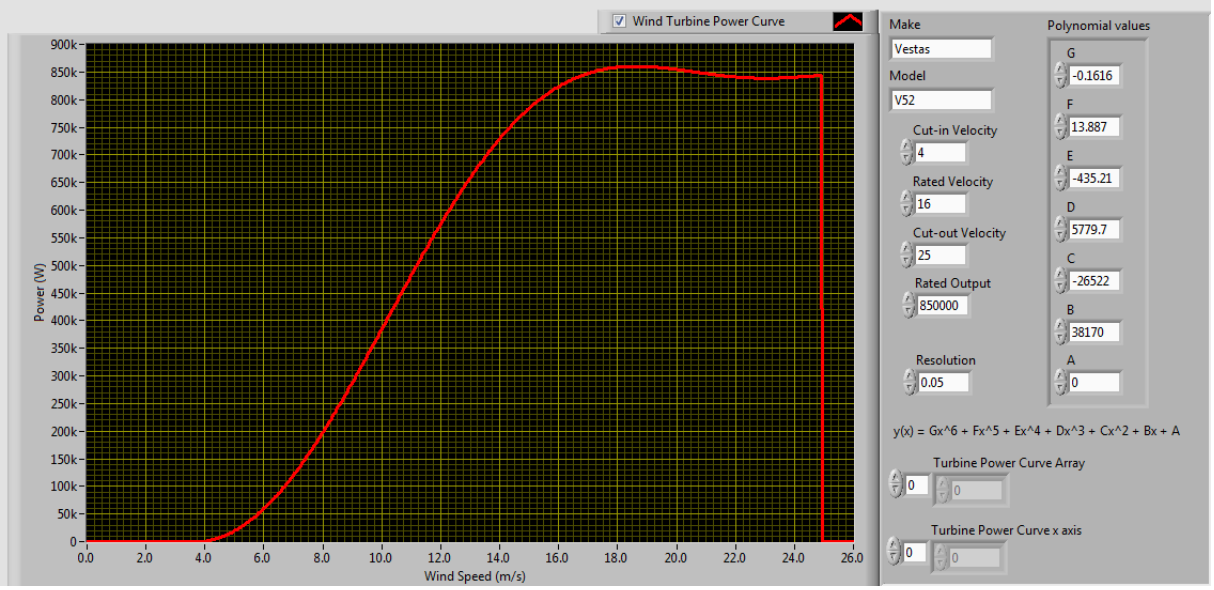

Figure 4.7: 6^{th} Order polynomial generated wind turbine power curve

4.1.6 Probable wind power output

Now that we have obtained a mathematical representation of the wind turbine's power curve as well as the probable wind speeds, we can calculate the probable power output of the wind turbine.

The first method entailed evaluating the polynomial in equation 4.2 using a for loop, for each month of the year, by substituting all the data values for said month into the polynomial and averaging the results. An excerpt of the Matlab code for this implementation is showed below:

```
v_ci = 4;
v_co = 25;

for month = 1:12
    for p=1:size(data(month).original)
        x = data(month).original(p);
        if (x >= v_ci)
            if (x <= v_co)
                pwrsum(p) = turbine.poly(x);
            end
```

```
            else
                pwrsum(p) = 0;
        end
    end

    data(month).pwrsum = pwrsum;
    pwrsum =[];

    meanpwr(month).sum  = mean(data(month).pwrsum);
plottemp(month) = meanpwr(month).sum;
end
```

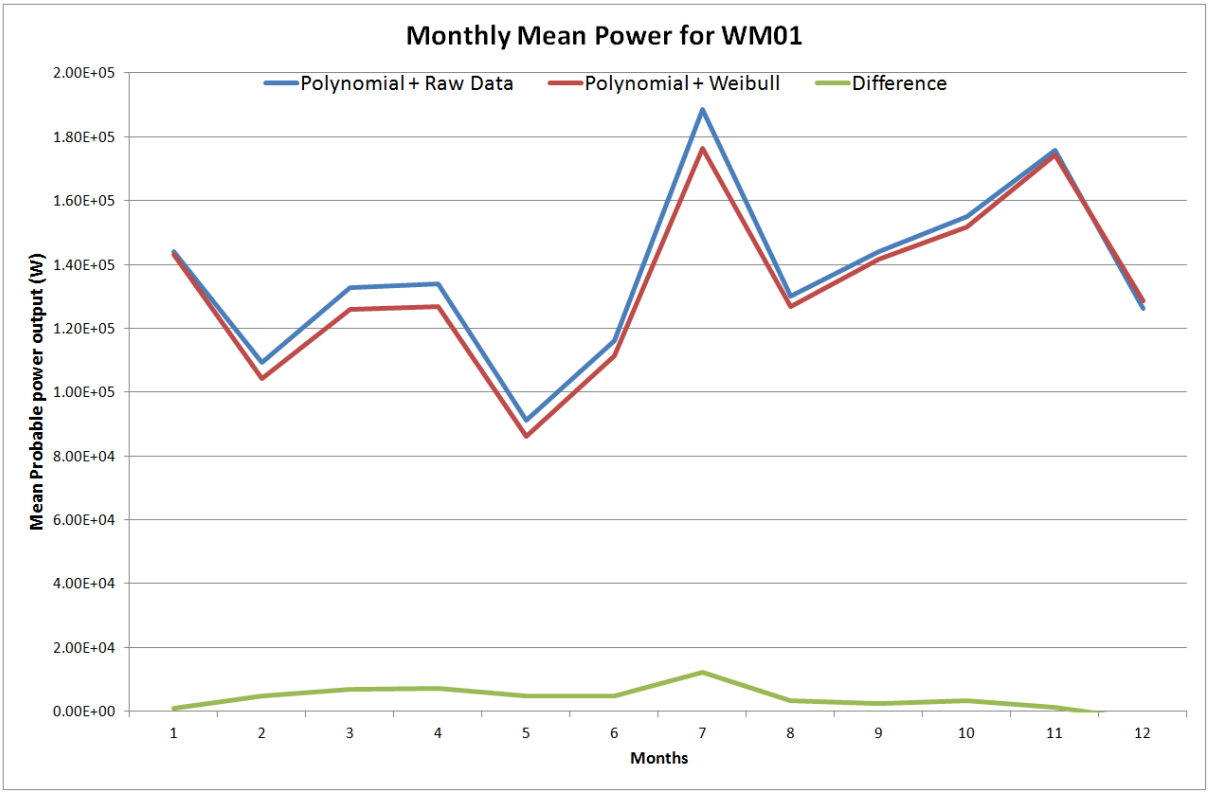

Figure 4.8: Monthly mean power outputs from LabView

resulting in the monthly mean power values graphed in figure 4.8. This is a cumbersome exercise to supply the wind speed entries for each month to equation 4.2, and averaging it. To put it into perspective, January alone contains 4464 data entries for which the polynomial has to be evaluated.

Figure 4.8 also contains the probable power outputs as calculated with the help of the

Weibull PDFs. The Weibull PDF representing the wind speed probabilities as well as the turbine's power curve can be seen in figure 4.9. The multiplication of these two curves produces a probable power output graph that represents the probability of the turbine producing a certain amount of power.

The integral of this probable power output curve resulted in the mean power value for the month in question. This calculation is much simpler than evaluating the polynomial for each data entry. If one were to evaluate a different wind turbine for the same site, one would only need to multiply the new power curve with the existing Weibull PDF, where as the polynomial substitution method would have to be repeated from the start.

As with any approximation one would expect a slight variance in the values. A detailed list of the power outputs obtained from Matlab and LabView, utilising the various methods, is provided in table 4.4. These variances from the polynomial power output for each method is expressed as a percentage value.

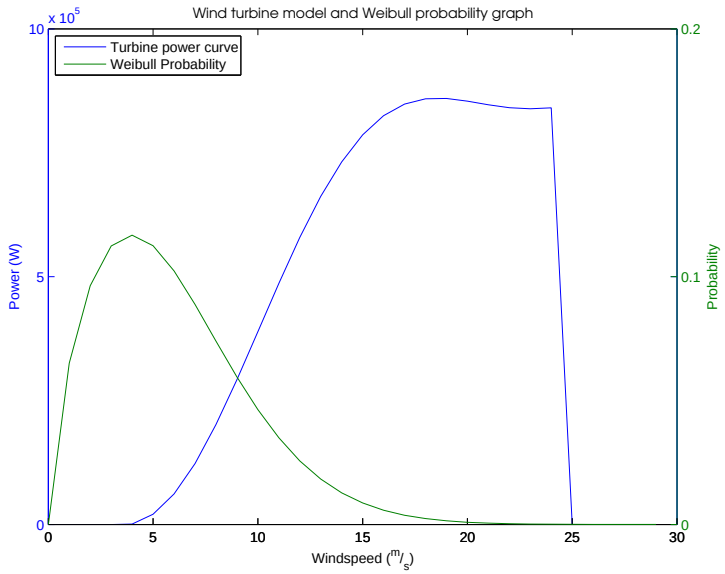

Figure 4.9: Wind turbine power curve alongside the Weibull PDF

Table 4.4: Mean monthly power output comparison

MONTHLY MEAN POWER OUTPUTS (W)							
MONTH	***MATLAB***			***LabView***			
	POLY	*MLE*	*Diff%*	*CFM*	*Diff%*	*MLE*	*Diff%*
Jan	**1.42E+05**	1.43E+05	0.12	1.27E+05	1.77	1.41E+05	0.10
Feb	**1.06E+05**	1.04E+05	0.26	1.06E+05	0.08	1.03E+05	0.43
Mar	**1.30E+05**	1.26E+05	0.47	1.09E+05	2.43	1.24E+05	0.68
Apr	**1.31E+05**	1.27E+05	0.45	1.21E+05	1.19	1.25E+05	0.69
May	**8.82E+04**	8.62E+04	0.23	7.47E+04	1.58	8.46E+04	0.42
Jun	**1.14E+05**	1.11E+05	0.35	1.12E+05	0.18	1.09E+05	0.53
Jul	**1.87E+05**	1.76E+05	1.24	2.20E+05	3.95	1.74E+05	1.50
Aug	**1.28E+05**	1.27E+05	0.09	1.15E+05	1.52	1.25E+05	0.34
Sep	**1.42E+05**	1.42E+05	0.00	1.36E+05	0.65	1.40E+05	0.26
Oct	**1.53E+05**	1.52E+05	0.17	1.42E+05	1.37	1.50E+05	0.45
Nov	**1.74E+05**	1.74E+05	0.03	1.65E+05	1.01	1.72E+05	0.19
Dec	**1.25E+05**	1.29E+05	0.51	1.05E+05	2.29	1.27E+05	0.22
AVERAGE			0.33		1.50		0.48

4.1.7 Battery bank

The battery bank module's calculations are fairly simple compared to the previous sections. This module assessed the system's power requirements in terms of the system bus voltage (v_{bus}) and total amount of power drawn from the battery bank (P_{dfb}). This module automatically obtains the amount of power supplied to the battery bank (P_{stb}) as calculated by the preceding wind and solar modules.

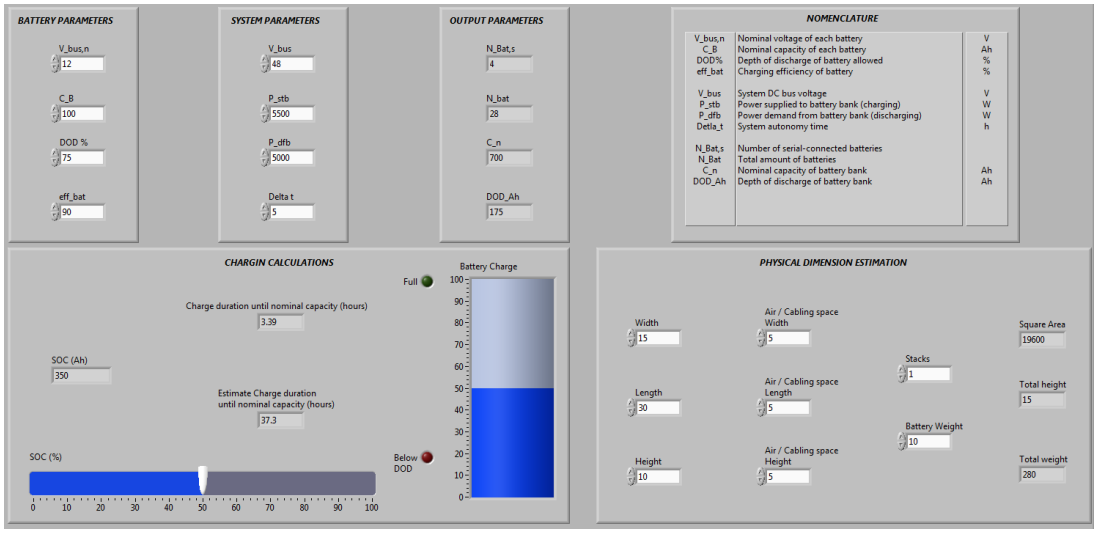

Figure 4.10: Screen capture of the battery bank user interface

Depending on the nominal capacity of the selected batteries, the module will determine how many batteries are required to achieve the required system autonomy time T_{days} as specified by the user. The user is further able to simulate the current state of charge SOC in order to investigate the charging duration of the batteries under full- and no-load conditions. This illustrates how long it will take to recharge the battery bank using the renewable energy sources if the batteries have been depleted to a certain SOC due to bad weather or system maintenance.

An additional panel allowed the user to estimate the physical dimensions of the battery bank. Although this seems to be a trivial exercise, the physical dimensions of a battery bank can be substantial, especially when low-capacity batteries are used.

4.2 Data resolution analysis

The data resolution analysis section does not fall within the project's scope, but was added to better understand the results and variations obtained during the simulations.

Throughout the duration of the project, special attention was devoted to any and all things related to the wind. This was due to the uncertainty regarding the data's resolution's effect on the simulations. This uncertainty was addressed by a method dubbed the dynamic resolution analysis simulation (DRAS). The DRAS required that every module pertaining to the wind analysis, be evaluated using a variable resolution data set. This variable resolution data set was created from the original data set where there was a data entry for every 10 minutes, by down-sampling and averaging the data entries every 20 minutes, 30 minutes, etc. up to a single data entry every 24 hours. This variable resolution data is illustrated in figure 4.11. The various resolutions R are calculated by

$$R = \lambda \cdot 10min \tag{4.3}$$

where λ is a scalar value ranging from $1 - 144$.

The results of the DRAS analysis proved enlightening as the effects of the the resolution on various aspects of the simulation became apparent. The first module affected by the resolution was the parameter estimation module. Figure 4.12 illustrates how the Weibull PDFs vary due to the different data resolutions. The MLE parameter estimation method relies on a multitude of data entries in order to converge on the most accurate parameters. As λ increases, the number of available data entries decrease by the same factor of λ, hence reducing the MLE iterations and ultimately resulting in a less accurate representation of the raw data set.

This effect is then compounded when using the Weibull PDFs, which is all ready an approximation of the actual wind speed, to calculate the probable power output of the wind turbines. The mean monthly power outputs for a wind turbine was calculated using the raw data where $\lambda = 1$, and repeated for each value of lambda. The results of these calculations can be seen in figure 4.13. There is a clear difference between the

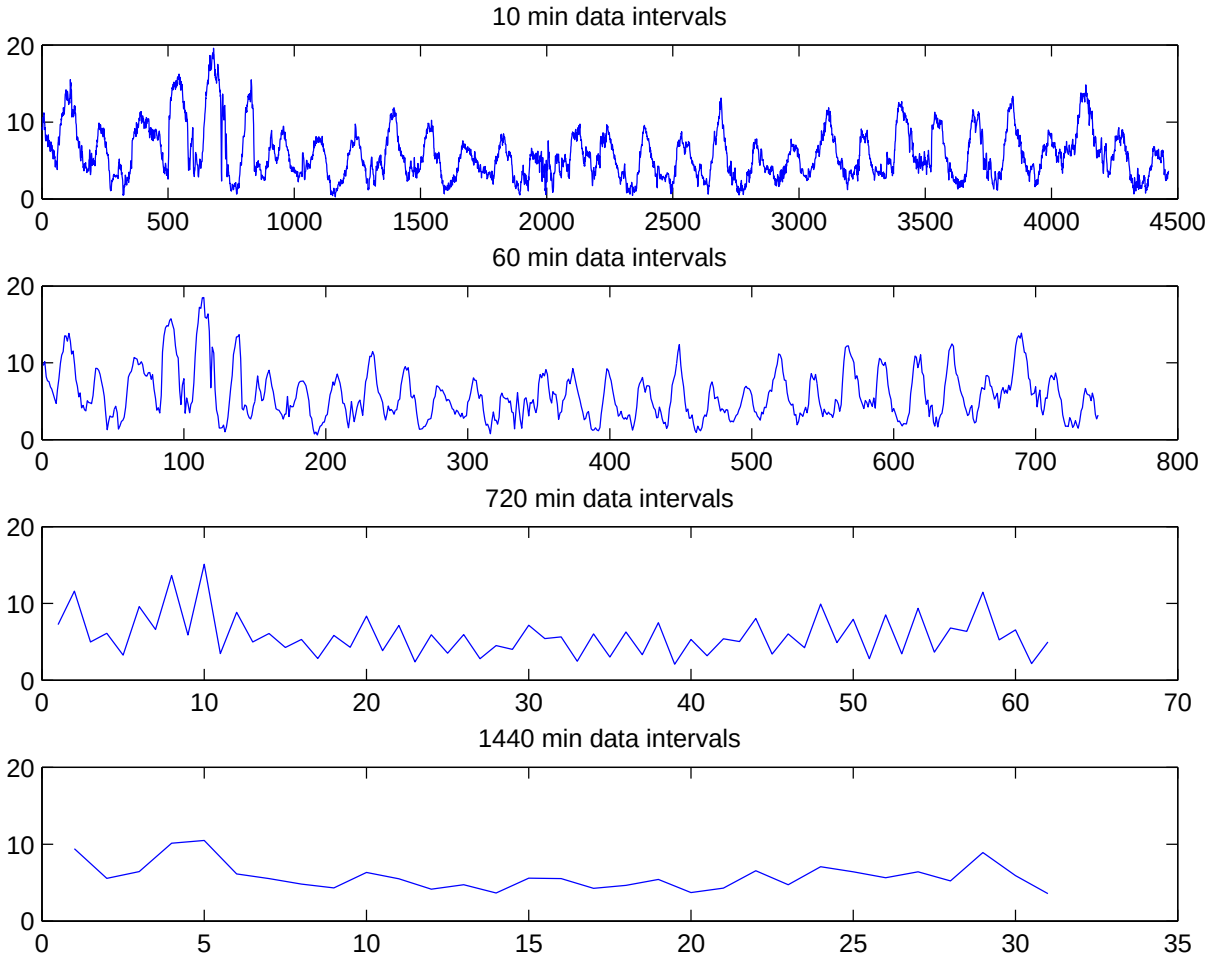

Figure 4.11: Monthly data representation for various sampling resolutions

mean power output in each month depending on the resolution, following an almost linear pattern. The coarser the data resolution, the lower the probable power output across all the months.

This fairly linear scaling effect of the resolution is better illustrated in figure 4.14 that displays the absolute value of the difference between the probable power calculated by direct substitution of $\lambda = 1$ data in to the turbine's power polynomial, and each subsequent resolution's Weibull PDF for $\lambda = 1$ (10 minutes) to 144 (24 hours). The finer resolution $(\lambda = 1)$ provided the best results with the smallest variation in power output.

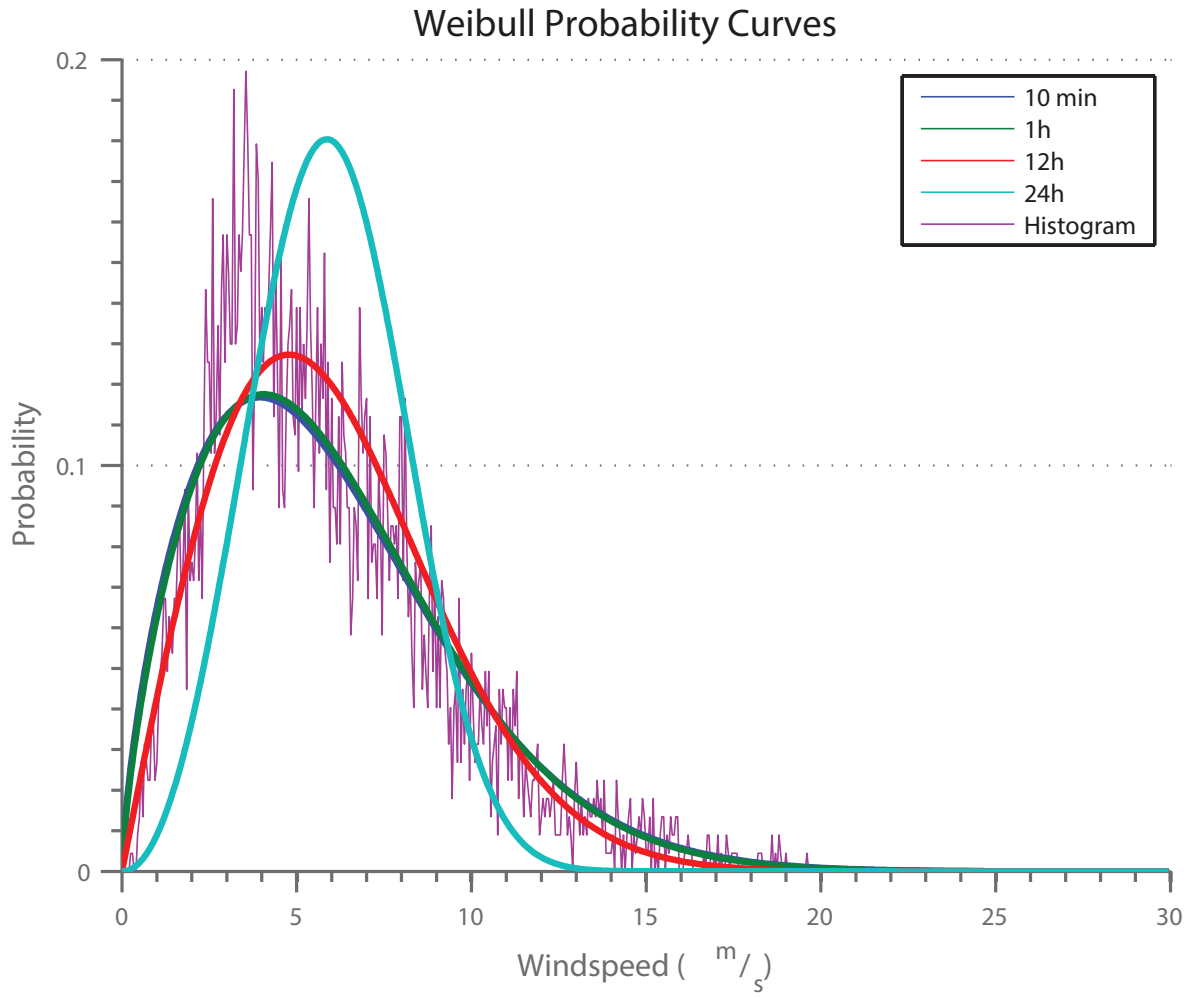

Figure 4.12: Resolution effects on Weibull probability curves

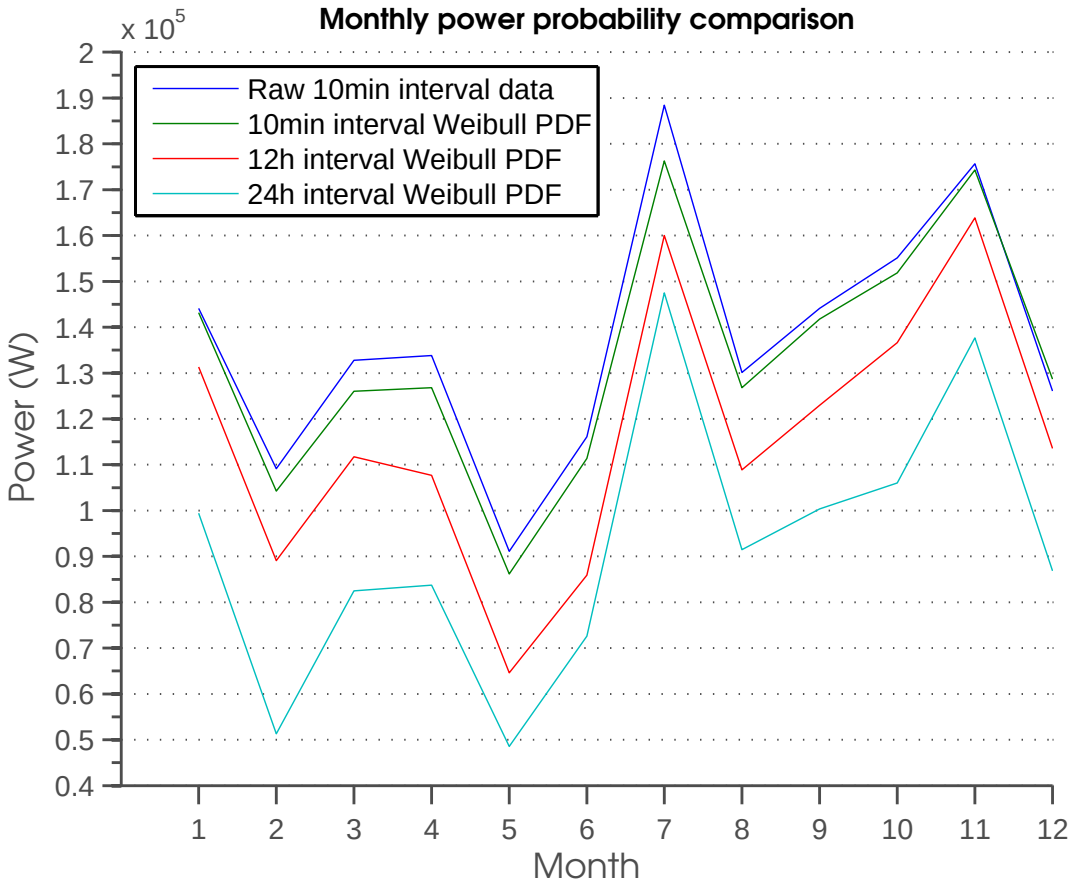

Figure 4.13: Monthly power probability comparison for various data resolutions

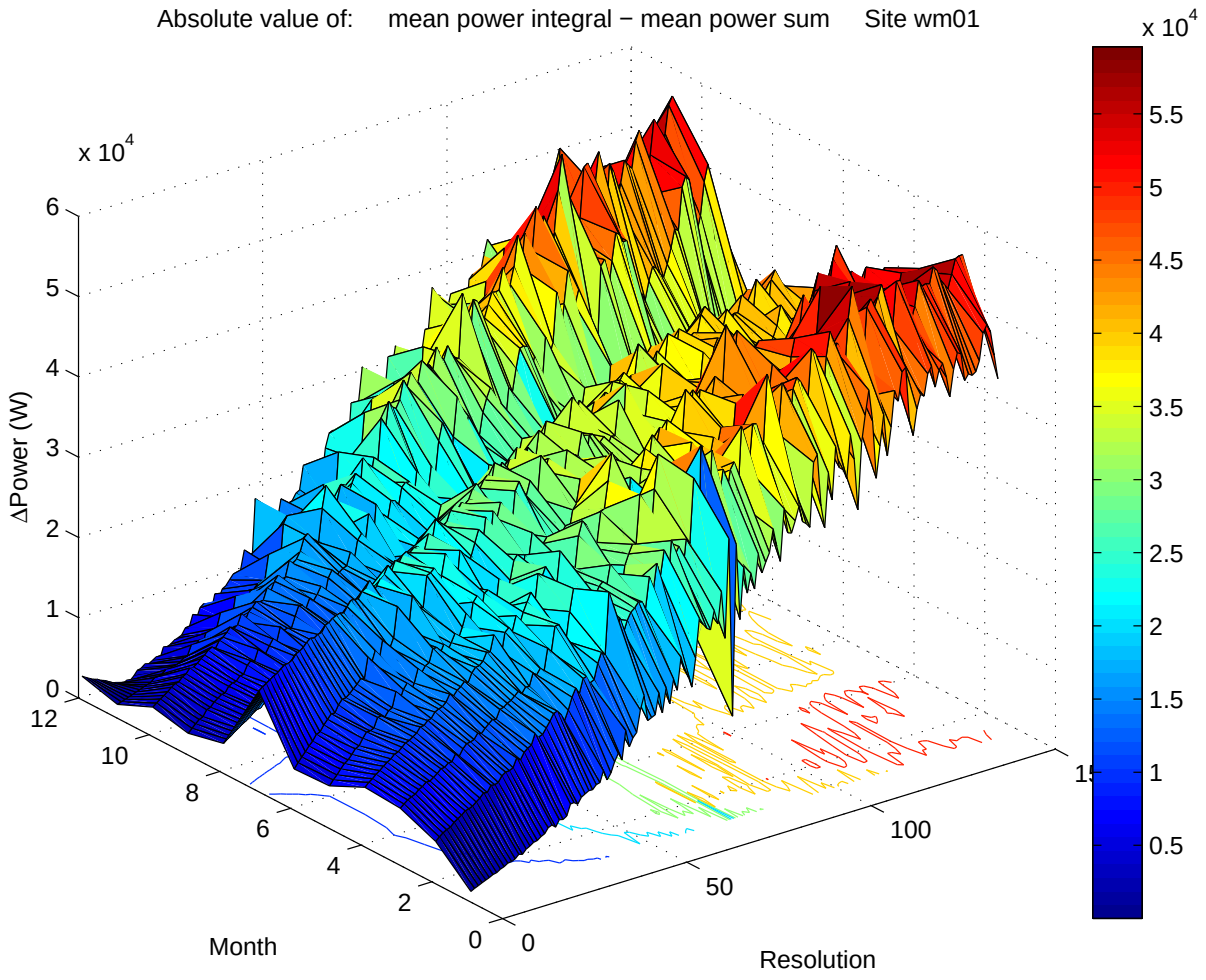

Figure 4.14: 3D Representation of the resolution's effects on the mean power calculations

By fitting a straight line through every month's difference plot, we were able to determine the average gradient of this linear characteristic due to the change in resolution. Figure 4.15 shows the difference plots for each month as well as the linear trend lines T:

$$T(\lambda) = m \cdot \lambda + C \tag{4.4}$$

where C is the y-axis offset constant and m is the gradient of the line. Table 4.5 contains the minimum, maximum and mean gradients calculated from the difference plots. The y-axis offset was chosen to be zero in order to provide a simplified indication of the linear trend of the mean power differences due to a corresponding change in resolution.

Table 4.5: Trend line gradients

TRENDLINE	*GRADIENT m*
Min	213.87
Mean	321.19
Max	405.84

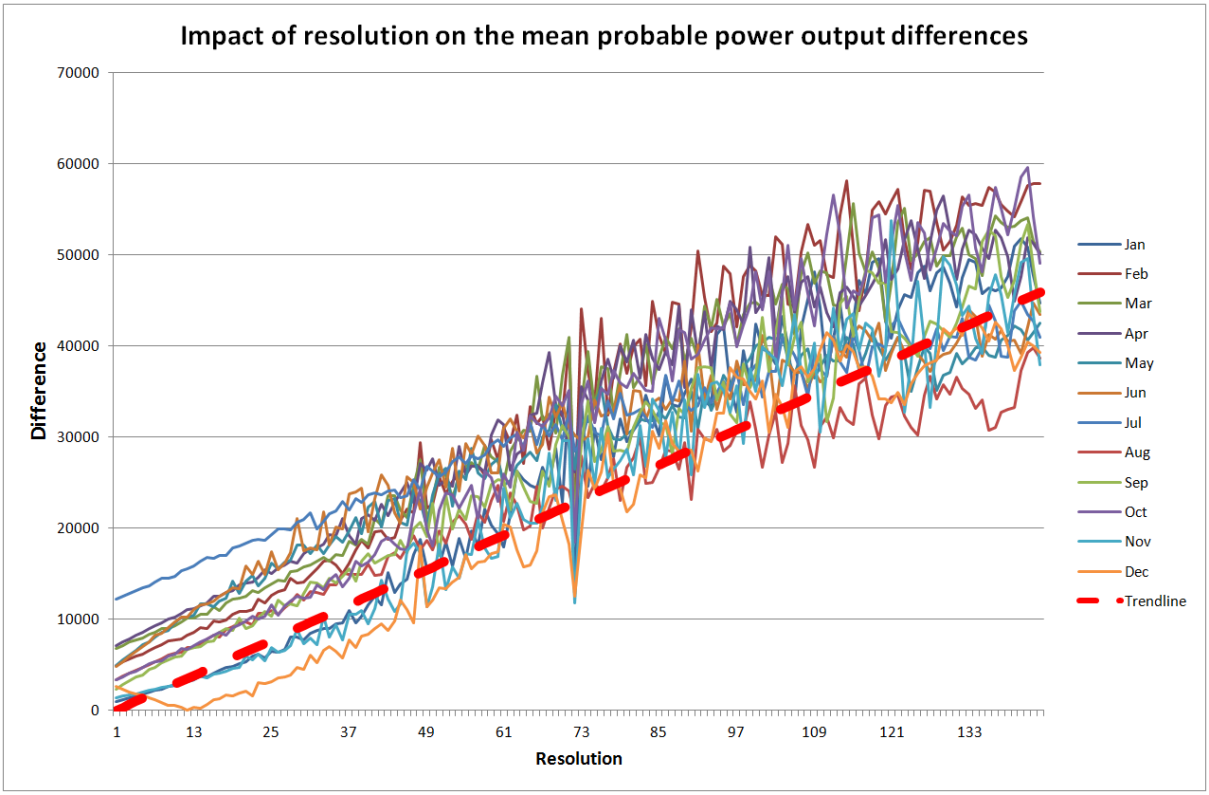

Figure 4.15: Differences in mean probable power output due to varying resolution

4.2.1 DRAS Anomaly

From figure 4.14 and figure 4.15 one can clearly see an anomaly at a resolution of $\lambda = 72$ and yet another small anomaly where $\lambda = 48$. After re-evaluation of the iterative algorithm, and using a different data set, similar results were obtained by the DRAS. A certain amount of seasonality in the wind data was to be expected, but after calculating the fast Fourier transform (FFT) of the raw data for various months, an interesting discovery was made. The FFT of the various months are overlaid in figure 4.16 to see if

there are any similarities between the different months. An excerpt of the Matlab code for this FFT is included in appendix A.1.

It is clear from figure 4.16 that there are some harmonics present in the data. The peak located at a frequency of 1 day was expected, but there seems to be a prominent harmonic at a frequency of 2 - i.e. every 12 hours. This correlates with the abnormality found in figure 4.9. Following this trend, it was expected to see yet another peak located at a frequency of 3 i.e. every 8 hours correlating with the abnormality at $\lambda = 48$, but there is too much noise on the graph to make a definitive call. Filtering of the raw data signals before the FFT, did not provide any noticeable improvement in the FFT graph.

As previously stated, the mean monthly power difference for the various resolutions are illustrated in figure 4.15. The anomaly at $\lambda = 72$ (12 hours) show a substantially lower deviation in the mean probable power output across all the months.

If the results obtained can be duplicated and verified while using data from a different source, one may draw the following hypothesis:

> The power output of a wind turbine generator is linearly related to the resolution of the data used for the calculations. If the probable power output P_λ for a wind turbine is known for a certain resolution λ_{known}, then one might be able to extrapolate a more accurate power output by using the linear relation between the power output and the data's resolution.
>
> By extrapolating a data set with a coarser resolution $(\lambda > \lambda_{known})$ from the original data set, one will be able to determine the probable power output from these new data sets. By doing this multiple times, one will obtain an array containing the probable power outputs for various resolutions. By determining the gradient M of the relation between these probable power output values, one can extrapolate the power output value at $\lambda = 1$, equivalent to a 10 minute sampling interval, by fitting a straight line with gradient M, through P_λ and evaluating it at $lambda = 1$.

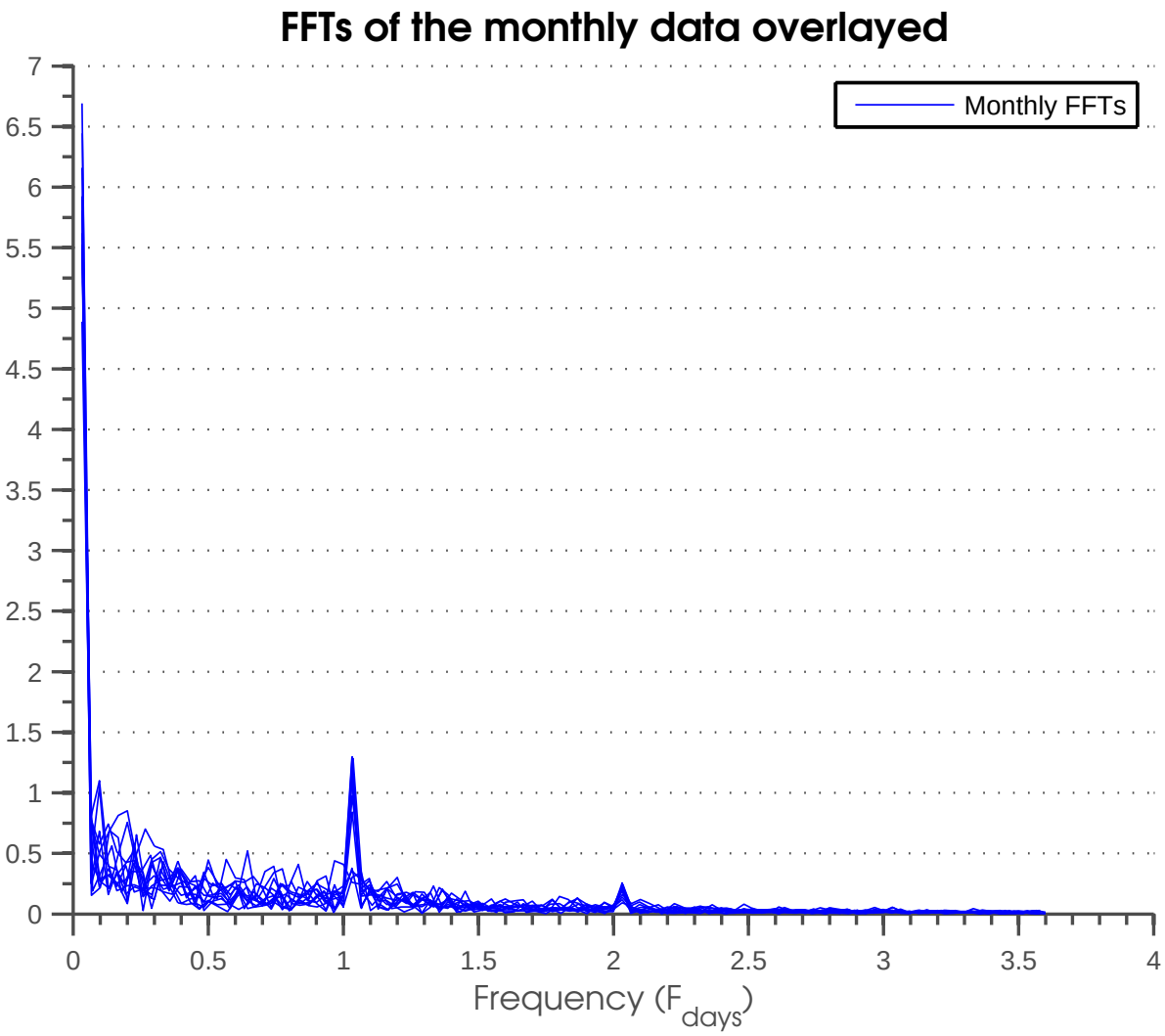

Figure 4.16: FFT

4.3 Integrated model results

By integrating this technical simulation model (TMS) with the economic simulation model (ESM) of Louw et al. [15], we were able to determine the optimal system configuration base to deliver the most power for the lowest cost. An in depth analysis of the integration can be found in the dissertation of Mr. Louw [15].